Available online at www.sciencedirect.com
SCIENCE DIRECT®
International Journal of Heat and Mass Transfer 47 (2004) 3257–3268
International Journal of HEAT and MASS TRANSFER
www.elsevier.com/locate/ijhmt

Microscale heat transfer measurements during pool boiling of FC-72: effect of subcooling

Fatih Demiray [a], Jungho Kim [b,*]

[a] Arcelik A.S., Eskisehir 26110, Turkey
[b] Department of Mechanical Engineering, University of Maryland, 2181 Glenn L Martin Hill, College Park, MD 20742, USA

Received 23 July 2003; received in revised form 6 February 2004
Available online 19 March 2004

Abstract

Heat transfer under nucleating bubbles were directly measured using a microheater array with 100 μm resolution with low and high subcooled bulk liquid along with images from below and from the side. The individual bubble departure diameter and energy transfer were larger with low subcooling but the departure frequency increased at high subcooling, resulting in higher overall heat transfer. The bubble growth for both subcoolings was primarily due to energy transfer from the superheated liquid layer-relatively little was due to wall heat transfer during the bubble growth process. Oscillating bubbles and sliding bubbles were also observed in highly subcooled boiling. Transient conduction and/or microconvection was the dominant heat transfer mechanism in the above cases. A description of the experimental setup, the results, and implications for modeling boiling heat transfer are presented. A transient conduction model is developed and compared with the experimental data.

Keywords: Boiling; Microheater array; Subcooling; Microconvection; Transient conduction

1. Introduction

The mechanisms by which bubbles transfer energy from a wall are actively being investigated experimentally and numerically. Many mechanisms for bubble heat transfer have been suggested (see Carey [1] for a short review) but the microconvection model of Mikic and Rosenhow [2] and the microlayer model of Cooper and Lloyd [3] are the most widely cited. Recently, a contact line model of bubble heat transfer has also been presented (e.g., Stephan and Hammer [4] and Mitrovic [5]). The large number of experimental studies to date have been supplemented recently by numerical simulations made possible by advances in computer hardware and interface tracking codes. Examples of recent numerical simulations include Welch [6], Son et al. [7], and Yoon, et al. [8]. The proliferation of competing bubble heat transfer models has primarily been due to the inability to make detailed measurements in the vicinity of the bubble.

Yaddanapudi and Kim [9] measured local heat transfer data underneath single bubbles nucleating periodically from a single site for saturated FC-72 at 1 atm ($T_{sat} = 56.7$ °C) and wall temperature 79.2 °C. They used a heater array with individual heaters 270 μm in size. The bubble departure diameter was about 370 μm, only slightly larger than a single heater. Their results indicated that bubble heat transfer mechanisms were different from the widely accepted view of microlayer evaporation being the dominant heat transfer mechanism in saturated pool boiling. Bubble growth occurred primarily due to energy gained from the superheated liquid layer. Bubble departure resulted in removal of part of the superheated layer, allowing energy to be transferred from the wall through transient conduction

* Corresponding author. Tel.: +1-301-405-5437; fax: +1-301-314-9477.
E-mail addresses: demirayf@yahoo.com (F. Demiray), kimjh@eng.umd.edu (J. Kim).

0017-9310/$ - see front matter © 2004 Elsevier Ltd. All rights reserved.
doi:10.1016/j.ijheatmasstransfer.2004.02.008

Nomenclature

A_h	area of heater
d_{eq}	equivalent diameter
f	frequency
h_{fg}	enthalpy
k	thermal conductivity
L	length
P	pressure
$\dot{q}$	power
$\dot{q}''$	heat flux
$\dot{q}''_h$	heat flux transferred from heater to liquid
q''_{raw}	heat flux supplied to heater
r	radius
r_i	minimum radius
r_0	initial radius
T	temperature
T_w	wall temperature
T_l	liquid temperature
t	time
v	velocity
w	width of heater
x	x-direction

Greek symbols

α_l	thermal diffusivity of liquid
ρ_v	density of vapor

and/or microconvection, consistent with the model of Mikic and Rosenhow [2].

Demiray and Kim [10] presented local heat transfer data underneath bubbles nucleating from a single site for single and vertically merging bubbles under conditions similar to Yaddanapuddi and Kim [9], but using an array with heaters 100 μm in size. The surface temperature of the heater array and the bulk fluid temperature during the experiment were 76 and 52 °C, respectively. Bubbles that nucleated at this site alternated between two modes: single bubble mode and multiple bubble mode. In the single bubble mode, discrete bubbles departed from the heater array with a waiting time between the departure of one bubble and nucleation of the following bubble. In the multiple bubble mode, bubble nucleation was observed immediately after the previous bubble departed. The departing bubble pulled the growing bubble off the surface prematurely and the bubbles merged vertically forming small vapor columns. The data indicated that the area influenced by a single bubble departing the surface was approximately half the departure diameter. Microlayer evaporation was observed to contribute a significant, but not dominant, fraction of the wall heat transfer in the single bubble mode. Microlayer evaporation was insignificant in the multiple bubble mode, and heat transfer occurred mainly through transient conduction/microconvection during liquid rewetting as the bubble departed the surface.

The objective of this work is to determine the mechanisms by which heat transfer occurs for bubbles nucleating from a single site, and extends the work of Yaddanapudi and Kim [9] and Demiray and Kim [10] to high subcooling. The array with microheaters 100 μm in size were used to obtain time and space resolved heat transfer measurements. A description of the experimental setup, the results, and implications for modeling boiling heat transfer are presented. A transient conduction model for the wall heat transfer is developed and compared with the data.

2. Experimental apparatus

2.1. Heater array

An array of 96 platinum resistance heater elements deposited on a quartz wafer provided local surface heat flux and temperature measurements. A photograph of the heater array is shown in Fig. 1. Each element in the

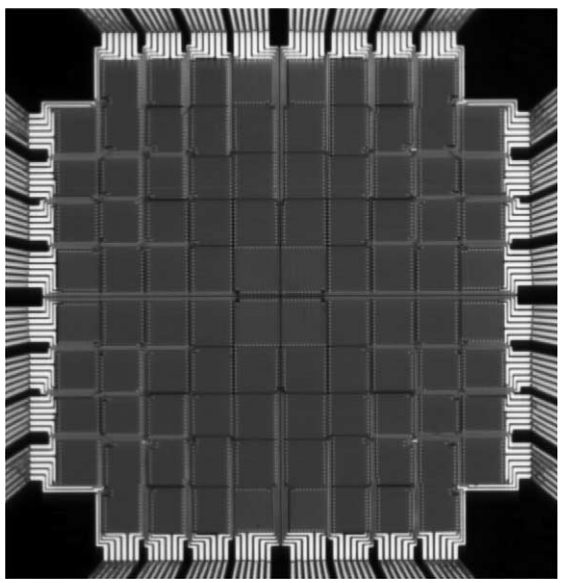

Fig. 1. Photograph of heater array.

array was approximately square in shape, nominally 0.01 mm^2 in area, and consisted of 2 μm wide Pt lines spaced 2 μm apart. Each heater had a nominal resistance of 8 kΩ with a temperature coefficient of resistance of 0.0019 $°C^{-1}$. The lines that supply power to the heaters are routed between the individual heaters and the PGA board. Details of the construction of a similar heater array are given in Rule and Kim [11].

2.2. Feedback control circuit

Each heater in the array was kept at constant temperature by individual feedback circuits similar to those used in hotwire anemometry—see Fig. 2 for a schematic of the circuit. Any imbalance in the Wheatstone bridge was sensed by an amplifier, which continually varied the power to the heater to bring the bridge back into balance. The output of the circuit was the voltage across the heater. The heat dissipated by a given heater could be calculated directly from this voltage and the heater resistance. The heater temperature was controlled by varying the wiper position of the digital potentiometer. The frequency response of the circuit was measured to be 15 kHz by measuring the response of the circuit to a step change in digital potentiometer position. Additional details regarding the electronics of the circuits is given in Bae et al. [12]. Because the individual heaters are quite a bit smaller than the bubble, the bubble sees, to a first approximation, a constant wall temperature boundary condition. On scales smaller than an individual heater, the boundary condition is neither constant wall temperature nor constant wall heat flux since the local temperature and power can change.

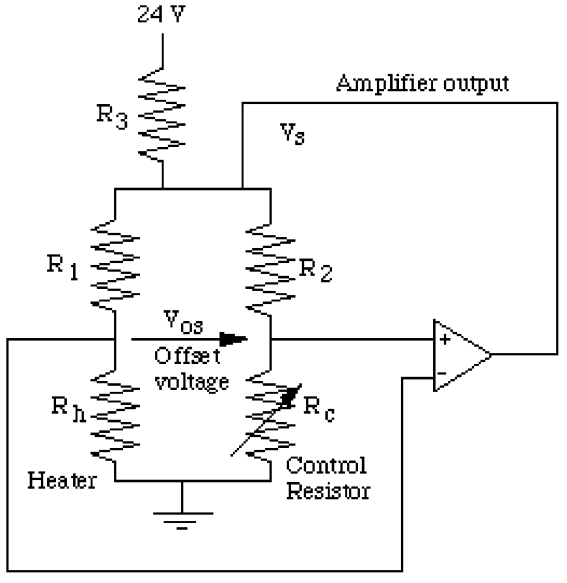

Fig. 2. A schematic diagram of the feedback control circuit.

2.3. Heater calibration

The heater array was calibrated in an oven held within 0.1 °C of the set temperature. Calibration consisted of finding the digital potentiometer wiper position that caused the feedback loop to just begin regulating for a given chamber temperature. Each heater in the array could be varied over a 120 °C range in 0.4 °C increments.

2.4. Data acquisition system

The two data acquisition cards (PCI-DAS6402/16), each capable of scanning 64 analog input channels at a maximum speed of 200 kHz, were installed inside a Dell OptiPlex GX110 computer. Each card sampled the outputs of 48 heaters. The system was used to obtain time-resolved data at 3704 Hz from each heater for a period of 4 s. Both data acquisition cards were triggered by the same rising edge of a TTL signal from the computer.

2.5. Boiling rig

The boiling rig shown in Fig. 3 was used in the experiments. The test chamber was filled with nominally 3 L of FC-72. The bellows and the surrounding housing allowed the test section pressure to be changed when needed. A stirrer was used to break up any stratification within the test chamber, while a series of thin film heaters attached to the outside of the chamber were used to control the bulk liquid temperature. The stirrer was turned off before the start of data acquisition to allow the bulk fluid motion to die out.

The fluid was degassed by repeatedly pulling a vacuum on the fluid. The final dissolved gas concentration in the liquid, determined using the chamber temperature and pressure, the properties of FC-72 (3M Fluorinert Manual [13]), and Henry's Law was less than 1.5×10^{-3} moles/mole.

2.6. High speed video

The semi-transparent nature of the heater array enabled images to be taken from below with a high-speed digital video camera (Vision Research Phantom IV) set to acquire 256×256 resolution images at 3704 fps. A group of high performance white LEDs was mounted over the heater array within the chamber in order to provide a bright, diffuse background for bottom-view pictures of the bubble. A second high-speed digital video camera (Vision Research Phantom IV) was used to record side-view images at the same speed and resolution. A halogen lamp next to a glass window in the boiling chamber provided light for side view images. Due to the heat produced by the lamp, the lamp was turned on only

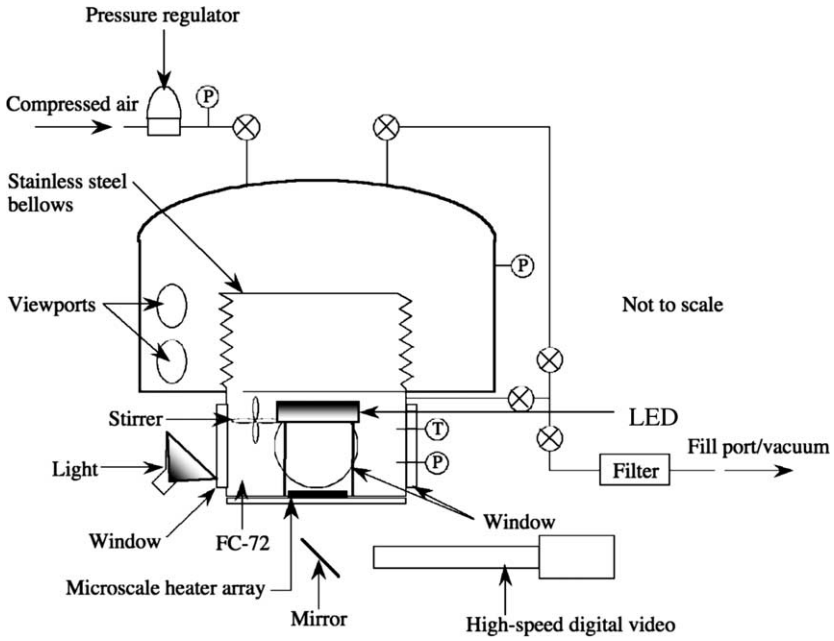

Fig. 3. Schematic of test apparatus.

during the data acquisition time. Recording of both cameras was initiated using the same signal used to trigger the data acquisition system, enabling heat transfer measurements and video records to be made simultaneously.

3. Data reduction and uncertainty analysis

Because each heater had its own feedback control circuit, we were able to measure the instantaneous heat flux required to maintain each heater at a constant temperature (q''_{raw}). Uncertainties in q''_{raw} are relatively small since they were computed directly from the measured voltage across the heaters and since the heater resistances do not change much. The maximum uncertainty in the voltage across the heater is 0.04 V. The uncertainty in heater resistance is about 45 Ω. Since the heater resistance is nominally 8 kΩ, the uncertainty in heater resistance is about 0.56%. The resulting uncertainty in heat transfer due to measurement inaccuracies in the feedback circuit and data acquisition system can be conservatively calculated to be less than 3%. Some of this power, however, is conducted from the heater elements to the quartz substrate and can eventually be lost by natural convection to the bulk liquid. In this study, we are interested in the heat transfer induced only by the bubble action. The heat transfer excursions around a slowly varying baseline were assumed to be due to bubble formation and departure. The baseline of the heat transfer curve exhibited a low frequency oscillation, which is likely due to natural convection flow over the heater driven by the temperature difference between the bulk liquid and the heater array. To obtain the effect of the bubble only, a sixth degree polynomial was fitted to selected points on the baseline and subtracted from the time-resolved heat transfer for each heater in the array. The resulting heat transfer curve could exhibit both positive and negative values. Negative values of heat transfer result if liquid dryout during bubble growth above a heater occurred, resulting in lower heat transfer than would have occurred in the case of natural convection in the absence of a bubble. If a functioning heater is next to a nonfunctioning heater (which acts as a local heat sink), the power required to keep it at constant temperature can change depending on the heat loss from the nonfunctioning heater, increasing the uncertainty. The total uncertainty due to uncertainties in substrate conduction, the curve fit, and nonfunctioning heaters is 0.2 mW for a single heater in the array. The uncertainty in the wall temperature is due to the limited resolution of the digital potentiometer, and is taken to correspond to two increments, or less than 1 °C.

An example of the data reduction is shown in Fig. 4, in which the total heat transferred from the array is obtained by summing the heat transferred from each heater together and plotted on the upper curve. Excursions in heat transfer above a slowly varying baseline are observed. These excursions correspond to a single or multiple bubble growth sequence from a single nucle-

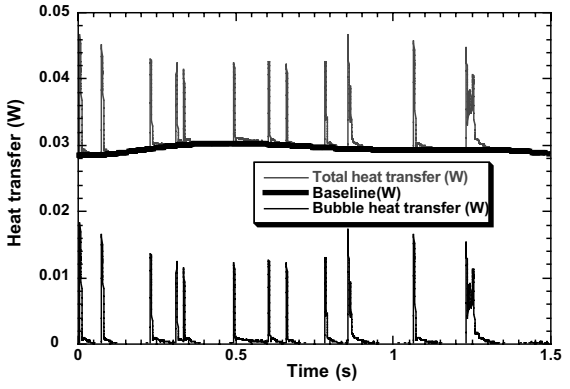

Fig. 4. Example of bubble heat transfer calculation.

ation site on the surface. The baseline obtained by a curve fit is overlaid on this curve. The lower curve was obtained by subtracting the baseline from the total heat transfer curve and is the net change in heat transfer due to the presence of the bubble on the surface.

4. Experimental results

All data were obtained with the wall temperature fixed at $T_{wall} = 76$ °C and $P = 1$ atm ($T_{sat} = 57$ °C). Two subcooling levels were investigated. The data taken with $T_{bulk} = 52$ °C will be referred to as low subcooling, while the data taken with $T_{bulk} = 41$ °C will be referred to as high subcooling.

4.1. Total heat flux

Heat transfer excursions from the baseline due to nucleating bubbles for both subcoolings are shown on Fig. 5. The low subcooling case consisted of single bubble events separated by relatively long waiting times with the exception of L10 (a double bubble event) and L13 (a triple bubble event). The reader is referred to Demiray and Kim [10] for a discussion of the heat transfer behavior for L10 and L13. The high subcooling case consisted of thirteen single bubble events (H1–H13) followed by a single bubble that oscillated on the surface (H14). A few trends are immediately evident. Bubble departure occurred much more frequently for high subcooling than low subcooling, consistent with the observations of other researchers (e.g., Forster and Grief [14]). The waiting time between bubbles for high subcooling was very short, and varied between 0 and 10 ms. The waiting time for low subcooling was much longer-between 0 ms and over 200 ms. Although the peak heat transfer for high subcooling was roughly two thirds that for low subcooling, the time averaged heat transfer for high subcooling was 3.5 vs. 0.98 mW for low subcooling due to the higher departure frequency.

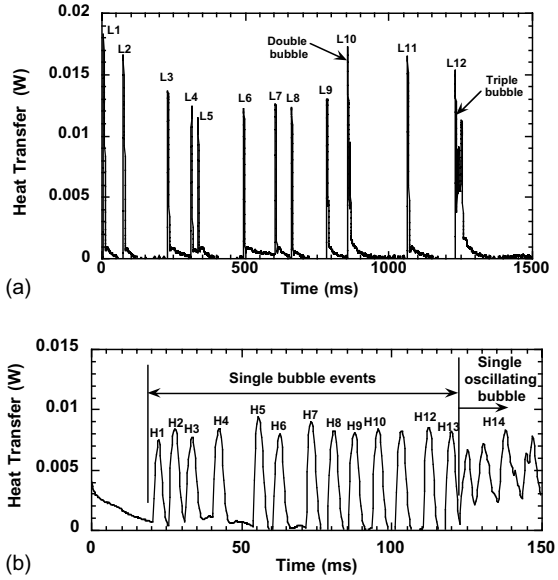

Fig. 5. Comparison of bubble heat transfer with low and high subcooling. Note the difference in time scales.

The heat transfer associated with single bubble events for both subcoolings are shown superimposed on each other on Fig. 6 where time for each bubble was shifted so that $t = 0$ corresponds to nucleation of the bubble on the surface. The low subcooling case shows an evolution from a double peaked heat transfer profile (bubbles L1–L4) similar to what was observed by Yaddanapuddi and Kim [9] and Demiray and Kim [10] to a profile with a single peak (bubbles L5–L9). Demiray and Kim [10] attributed the first peak at ~1.2 ms for bubble L1 to evaporation of a thin microlayer trapped between the growing bubble and the heated wall as the bubble grows nearly hemispherically in a superheated liquid layer. The

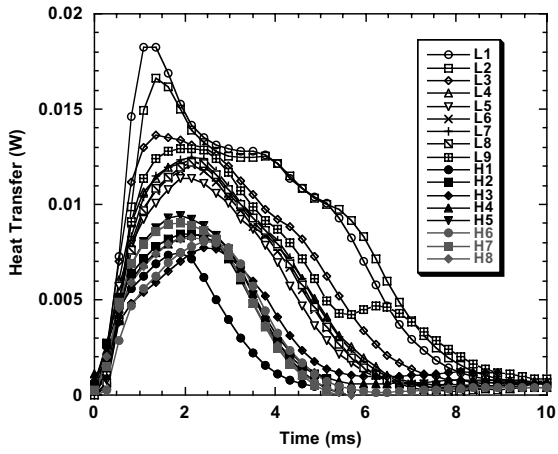

Fig. 6. Bubble heat transfer for low and high subcooling.

reason for the evolution from this profile to that observed for bubbles L5–L9 is unclear, but may be due to fluctuations in the temperature of the superheated liquid layer. Evidence for this is seen in the unreduced heat transfer data shown on Fig. 4. The magnitude of the excursion above the baseline heat transfer (recall that the baseline heat transfer is a measure of the substrate conduction plus natural convection) in this plot does not appear to correlate with the waiting time between bubbles, but does seem to be inversely correlated to the magnitude of the baseline heat transfer. Because the substrate conduction is nominally constant, an increase in the baseline heat transfer is indicative of a decrease in the local liquid temperature due to natural convection. The highly subcooled heat flux profiles have a shape similar to those for bubbles L5–L9, but with smaller magnitude. This seems to indicate that the rapid rise in heat transfer upon bubble nucleation (and therefore significant microlayer evaporation) resulting in a double peaked profile (bubbles L1–L4) occurs only when the bulk liquid is significantly superheated or if the superheated layer is sufficiently thick.

4.2. Space and time resolved heat transfer

Images showing the evolution of the bubbles for bubble Ll and H5 are shown on Fig. 7. Each heater in the array has been colored according to the heat transfer. The heat transfer behavior for each of these bubbles is discussed below.

Bubble L1 was discussed in Demiray and Kim [10], so only a brief summary is given here. Nucleation occurred between 0 and 0.27 ms. Based on the bottom view images, the bubble grew to nearly full size by 1.89 ms after nucleation. The bubble shape seemed to be approximately hemispherical. A large increase in the heat transfer under almost the entire bubble was observed during this time, consistent with evaporation from a microlayer between the bubble and the wall. Starting from 2.16 ms, the development of a low heat transfer region at the center of the bubble is observed, indicating progressive dryout of the microlayer. The dry spot size, as evidenced by the inner circle, reaches a maximum around 3.51 ms. The bubble began to depart the surface at this time, and the dry spot shrinks as the bubble necks down. Higher heat transfer is observed on the center heaters as they were rewetted by the bulk liquid. Bubble departure occurred at 5.13 ms, and is associated with a spike in heat transfer at the center heaters that decays with time.

The images for bubble H5 (subcooled case) are shown on Fig. 7(b). It is immediately apparent from these images that the maximum diameter of the bubble is much smaller than for the low subcooling case. The heat transfer behavior is similar to that observed for bubble L5. An apparently hemispherical bubble grows shortly after nucleation and high heat transfer is observed, indicating the formation of a microlayer. The heat transfer at the center of the bubble begins to decrease starting about 0.81 ms, and reaches a minimum at 2.16 ms indicating dryout of the microlayer. The heat transfer at the center of the heater begins to increase as the dark inner ring shrinks, indicating rewetting of the heater before bubble departure at 2.7 ms.

4.3. Measured and equivalent diameter

The wall heat transfer data shown in Fig. 6 can be used to compute an equivalent bubble diameter (d_{eq}) by assuming that all the heat transferred from all of the heaters goes into latent heat, Eq. (1).

$$\rho_v \frac{\pi d_{eq}^3(t)}{6} h_{fg} = \int_0^t \dot{q}_h''(t) A_h \, dt \tag{1}$$

where time $t = 0$ is assumed to be the start of nucleation for a single bubble. A plot of the time varying physical bubble diameter was obtained by fitting a circular template to the outer dark ring of the bubbles shown in Fig. 7, and is assumed to be a measure of the bubble volume. The equivalent diameter is plotted along with the physical diameter in Fig. 8 for representative single bubbles at low and high subcoolings. If the bubble were actually a hemisphere (approximately true for the bubble just after nucleation) instead of spherical (bubble shape close to departure), then the bubble diameter as measured above would be about $2^{1/3} = 1.26$ larger than the diameter of a spherical bubble of the same volume. The slight decrease in measured physical diameter after about 0.8 ms for bubbles L5 and L6 to about 91% of the maximum bubble diameter is most likely due to a transition from a hemispherical shape to a spherical shape as the bubble grows on the heater. A similar decrease in measured physical diameter at departure to about 84% of the maximum diameter is also observed for bubbles H5 and H6, and may be due to transition between a hemispherical to spherical shape as well as condensation at the top of the bubble. It is seen that d_{eq} is significantly smaller than the physical bubble diameter during the bubble growth time, indicating that the heat transferred from the wall cannot account for the bubble growth alone. For example, bubbles L5 and L6 reach a diameter of 0.5 mm $\times$ 0.54 ms. If a hemispherical bubble shape is assumed during this early bubble growth period, the diameter of a spherical bubble of equivalent volume is 0.4 mm. This is over twice as large as the d_{eq} derived from the wall heat transfer measurements at the corresponding time, indicating that the wall heat transfer could have contributed at most $1/2^3$ or 12.5% of the energy required to produce the bubble. The bubble must have gained the rest of its energy from the superheated liquid layer surrounding the bubble. The superheated

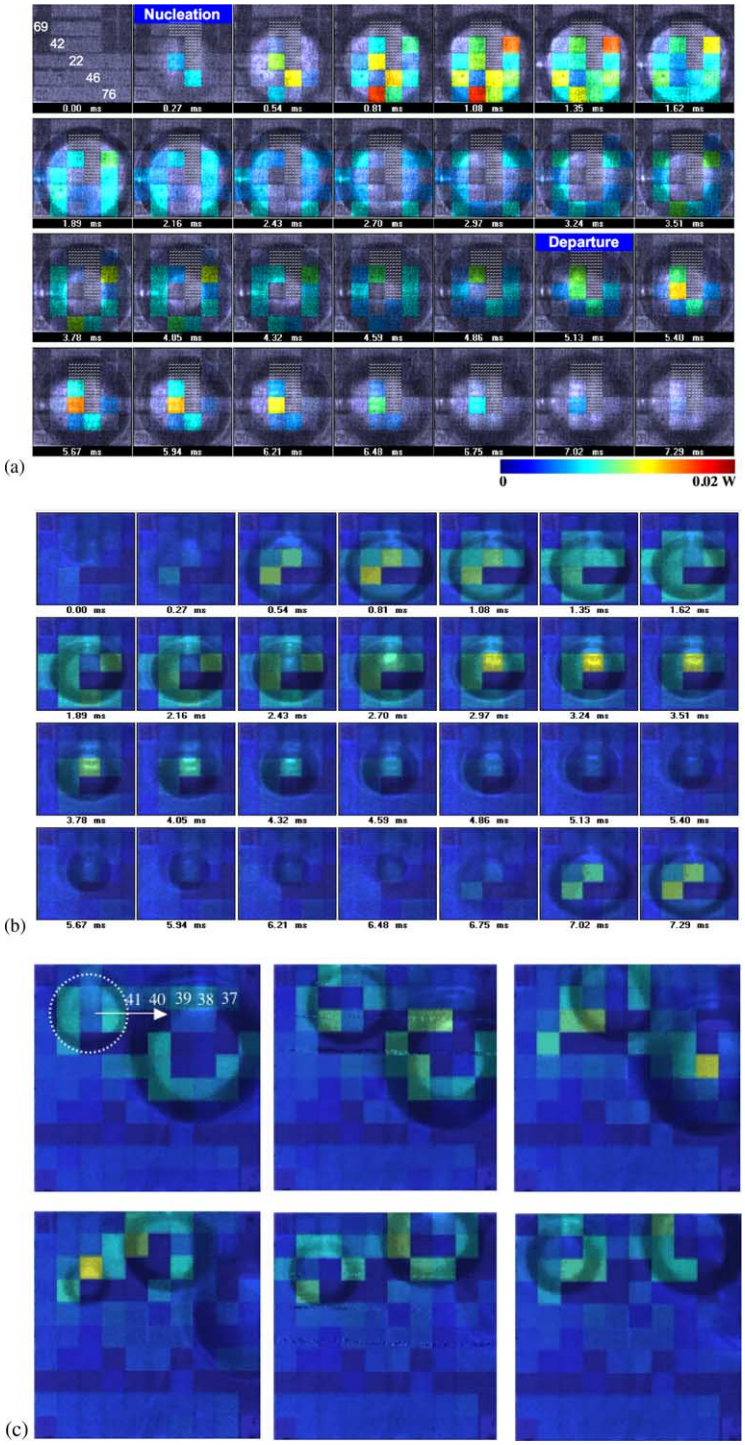

Fig. 7. Heat transfer distribution under (a) bubble L1, (b) bubble H5, bubble departure occurs 2.7 ms after nucleation and (c) a sliding bubble, successive images shown are left to right, top to bottom. The time between each image is 5.40 ms.

liquid layer acts as a reservoir of energy which the bubble draws upon during its growth. Conduction and microconvection during bubble growth and after it departs are the mechanisms through which this energy is replenished. This conclusion is consistent with the results of the study performed by Yaddanapuddi and Kim

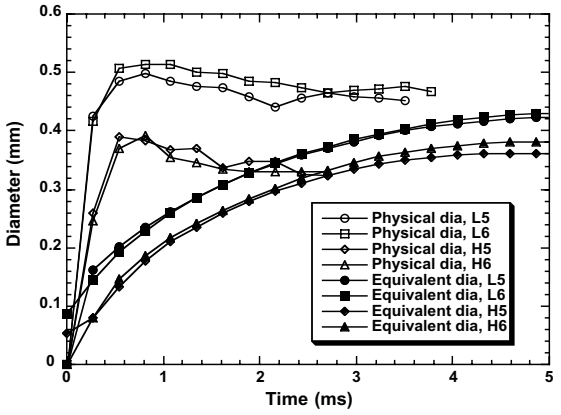

Fig. 8. Comparison of physical and equivalent bubble diameters.

[9] and Demiray and Kim [10]. Similar conclusions can be drawn from bubbles H5 and H6 in the high subcooling case.

The bubbles in the high subcooling case are significantly smaller than those in the low subcooling case since the thinner superheated liquid layer in the high subcooling case is not able to sustain growth of as large a bubble. The lower temperatures and thinner superheated layer in the highly subcooled case also cause the bubble to grow more slowly, limiting the amount of liquid trapped between the bubble and wall to form a microlayer. Increased condensation at the top of the bubble also acts to limit the bubble size.

4.4. Bubble heat flux

The heat fluxes under two bubbles for the high and low subcooling cases obtained by dividing the time resolved heat transfer by the time resolved bubble projected area are shown on Fig. 9. The heat fluxes for the high subcooling case are lower than those for the low subcooling case until about 1 ms, after which it increases substantially above it. It is interesting to note from the space resolved measurements (Fig. 7(a) and (b)) that the contact line diameter begins to decrease starting from about 1 ms. The higher heat flux for the highly subcooled case after this time in Fig. 9 is indicative of colder liquid rewetting the surface, resulting in higher transient conduction.

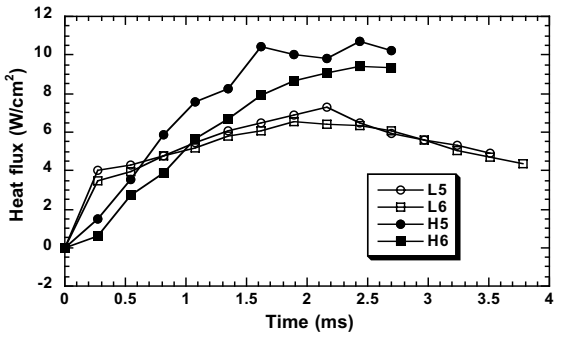

Fig. 9. Bubble heat flux variation for low and high subcooling.

4.5. Sliding bubbles, highly subcooled case

A particular bubble in the highly subcooled case was observed to slide along a line of heaters (41–38) as shown in Fig. 7(c). The time between each image is 5.40 ms, and the diameter of the bubble varied between 330 and 430 μm during this time. The dry patch size (taken to be the inner diameter of the dark ring under the bubble) varied between 240 and 290 μm. A given heater on this line first experiences natural convection, a receding contact line as the bubble moves over the heater, dryout, an advancing contact line as rewetting of the heater occurs, then the thermal wake behind the bubble. The heat transfer for the line of heaters is shown in Fig. 10. The peak receding contact line heat transfer is relatively constant for all five heaters and averages about 1.2 mW, or 12 W/m if the contact line length across a heater is estimated to be the width of the heater. The heat transfer decreases to near zero as dryout occurs, then increases again during the rewetting process. The peak heat transfer during rewetting is highest for heater 41 then decreases for successive heaters. It is expected from contact line theory that the heat transfer under a receding contact line (smaller contact angle) would be higher than under an advancing contact line (larger contact angle) if liquid flow to the meniscus were not limited. However, the heat transfer under the advancing contact angle is observed to be much higher than under the receding contact angle, contrary to what would be expected from contact line theory. This indicates an

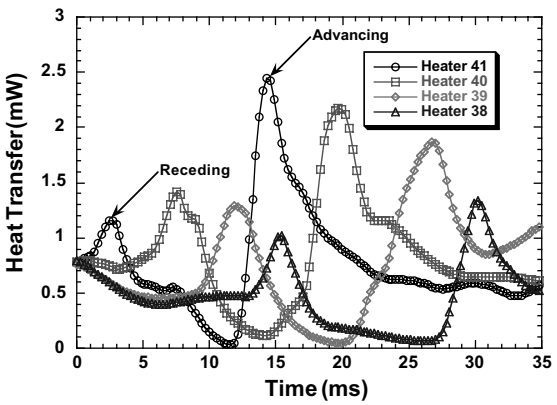

Fig. 10. Heat transfer from individual heaters during bubble sliding event.

additional heat transfer mechanism for the advancing contact line.

4.6. Oscillating bubbles, highly subcooled case

A single bubble in the highly subcooled case was observed to grow and shrink numerous times on the surface (bubble H14) before eventually departing. The projected outer diameter of the bubble along with the apparent diameter of the inner contact line obtained by fitting a circular template to the bottom view images is plotted in Fig. 11 along with the wall heat transfer. The size of the projected bubble diameter oscillated in size while growing steadily larger. The oscillatory bubble motion is caused by the bubble growing within the superheated layer then shrinking as condensation occurs over the bubble cap as it grows beyond the superheated layer into the colder bulk liquid. The liquid in the vicinity of the bubble becomes heated as the bubble oscillates, increasing the thickness of the superheated layer and resulting in a steady increase in the maximum bubble diameter. Bubble departure occurred at 50.2 ms shortly after the last oscillation on Fig. 11. The inner contact line diameter oscillates in phase with the projected diameter, but the magnitude of the fluctuation is larger.

The heat transfer is seen to vary inversely with the projected bubble diameter and the inner contact line diameter (i.e., the heat transfer decreases as the bubble grows and the contact line recedes, and increases as it shrinks and the contact line advances), indicating that the wall heat transfer does not govern the bubble behavior. Heat can be transferred from the wall to the fluid for the oscillating bubble through evaporation at the contact line or through transient conduction/microconvection to the bulk liquid. Since higher heat transfer occurs when liquid rewets the wall, transient conduction and/or microconvection appears to be the dominant mode of heat transfer for the oscillating bubble as well.

5. Advancing contact line heat transfer model description and validation

The experimental data discussed in this paper indicate that transient conduction/microconvection during liquid rewetting of the surface account for most of the wall heat transfer. A transient conduction model for advancing contact line heat transfer is developed next.

5.1. Linear contact line

Consider the case of a one-dimensional liquid front rewetting a heater that is at constant temperature T_w as shown in Fig. 12. It is assumed that the heat transfer at the three-phase line is negligible. The velocity of the liquid front is assumed to be v. The liquid is at temperature T_l far from the wall. If we assume 1-D conduction into the liquid, the heat flux at any position covered by liquid is obtained from the solution for transient conduction into a semi-infinite solid:

$$\dot{q}'' = \frac{k(T_w - T_l)}{\sqrt{\pi \alpha_l t}} \tag{2}$$

where t is the length of time the liquid has been covering a particular location on the heater. The heat transfer from the heater is given by

$$\dot{q} = \int_0^x \dot{q}'' w \, dx \tag{3}$$

where w is the dimension of the heater normal to the page and x is the position of the liquid front on the heater.

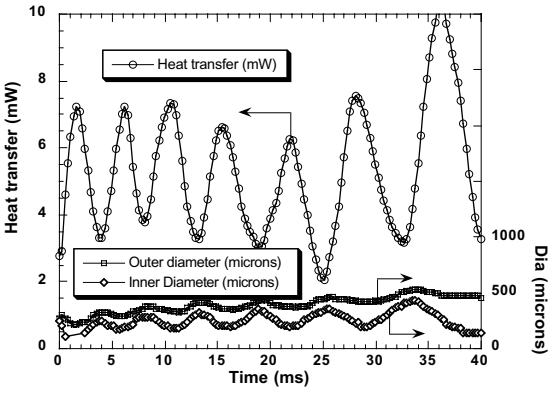

Fig. 11. Heat transfer variation for oscillating bubble H14 along with bubble size.

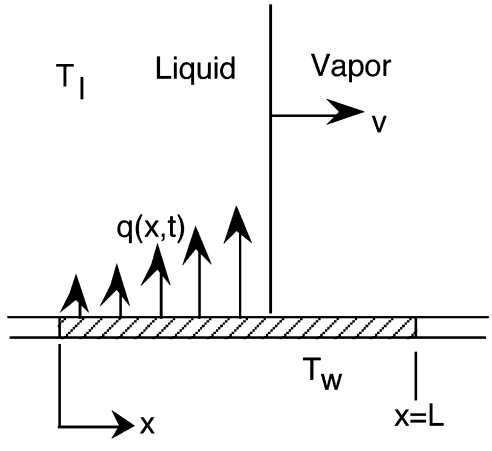

Fig. 12. Transient conduction model.

For the special case of a liquid front moving at constant velocity, $t = x/v$, the above equations can be combined to obtain the wall heat transfer to obtain

$$\dot{q} = \int_0^x \frac{k(T_w - T_l)\sqrt{v}}{\sqrt{\pi\alpha_l x}} w\,dx = \frac{2k(T_w - T_l)}{\sqrt{\pi\alpha_l}} w\sqrt{vx} \tag{4}$$

Transforming back to time coordinates yields

$$\dot{q}(t) = \frac{2k(T_w - T_l)}{\sqrt{\pi\alpha_l}} wv\sqrt{t} \tag{5}$$

The wall heat transfer at a given time for this simple case is observed to be proportional to the rewetting velocity (v) and increases with $t^{1/2}$. The peak heat transfer occurs just as the heater is completely rewet, and is given by

$$\dot{q} = \frac{2k(T_w - T_l)}{\sqrt{\pi\alpha_l}} w\sqrt{vL} \tag{6}$$

where L is the width of the heater.

The more general case where liquid always moves in the positive x-direction, but with variable velocity is considered next. Assume the time at which the liquid front reaches a particular position, $t = f(x)$, is known from measurements. It is desired to determine the wall heat transfer vs. time. The length of time a certain position x' has been covered with liquid when the front reaches a position $x > x'$ is given by

$$t - t' = f(x) - f(x') \tag{7}$$

The heat flux at position x' at time t is

$$\begin{aligned}\dot{q}''(x',t) &= \frac{k(T_w - T_l)}{\sqrt{\pi\alpha_l}} \frac{1}{\sqrt{t - t'}} \\ &= \frac{k(T_w - T_l)}{\sqrt{\pi\alpha_l}} \frac{1}{\sqrt{f(x) - f(x')}}\end{aligned} \tag{8}$$

The wall heat transfer at this time is then

$$\dot{q} = \int_0^x \frac{k(T_w - T_l)}{\sqrt{\pi\alpha_l}} \frac{1}{\sqrt{f(x) - f(x')}} w\,dx' \tag{9}$$

What happens after the liquid completely wets a heater of length L? The length of time a certain position x' has been covered with liquid at time $t > f(L)$ is given by $t - t'$ and the heat flux at x' is

$$\dot{q}''(x',t) = \frac{k(T_w - T_l)}{\sqrt{\pi\alpha_l}} \frac{1}{\sqrt{t - f(x')}} \tag{10}$$

To evaluate this further, consider the special case where the heat transfer from a heater is desired after it has been wetted by a liquid front moving with constant velocity, v. This is equivalent to the case where a liquid front wets the entire heater, then continues wetting the surface adjacent to the heater with the same velocity. We are only interested in the heat transfer between $x = 0$ and $x = L$, however. Suppose the liquid front is at position $x_t = L$. The wall heat transfer is given by

$$\dot{q} = \int_0^L \frac{k(T_w - T_l)}{\sqrt{\pi\alpha_l}} \frac{1}{\sqrt{f(x_t) - f(x')}} w\,dx' \tag{11}$$

Substituting $f(x_t) = x_t/v$ and $f(x') = x'/v$ yields

$$\dot{q} = \int_0^L \frac{k(T_w - T_l)}{\sqrt{\pi\alpha_l}} \frac{\sqrt{v}}{\sqrt{x_t - x'}} w\,dx' \tag{12}$$

Performing the integration and transforming back to time using $x_t = vt$ yields

$$\dot{q}(t) = \frac{2k(T_w - T_l)wv}{\sqrt{\pi\alpha_l}} [t^{1/2} - (t - L/v)^{1/2}] \tag{13}$$

The heat flux is observed to decay according to $t^{1/2}$.

Comparison of the transient conduction model to the sliding bubble case was performed for liquid rewetting heaters 41, 40, and 39. Liquid FC-72 at the bulk temperature (41 °C) wets the heaters at 76 °C. The average rewetting velocity for each heater was obtained from the measured position of the advancing contact lines vs. time (Fig. 13). Properties were evaluated at the saturation temperature. The comparison between the model and the measured heat transfer shown on Fig. 14 indicates that the model tracks the both the magnitude and trends of the measured data remarkably well for heaters 41 ($v = 3.7$ cm/s) and 40 ($v = 3.6$ cm/s). The agreement is not as good for heater 39 ($v = 2.1$ cm/s), and may be due

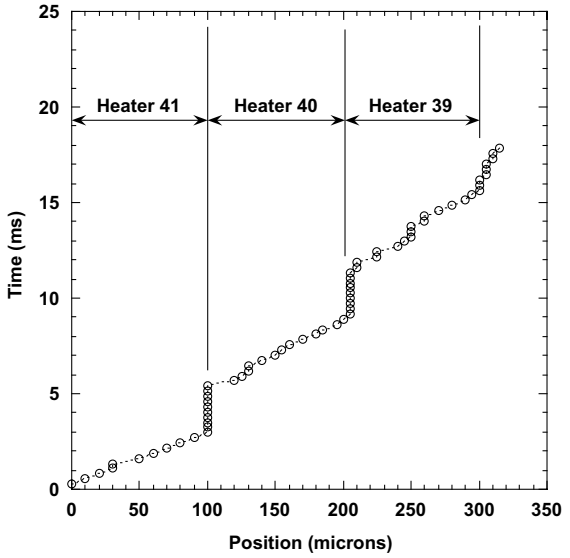

Fig. 13. Position of the advancing contact line on the heater. The bubble moves in the x-direction, and the 0-position is the left side of heater 41.

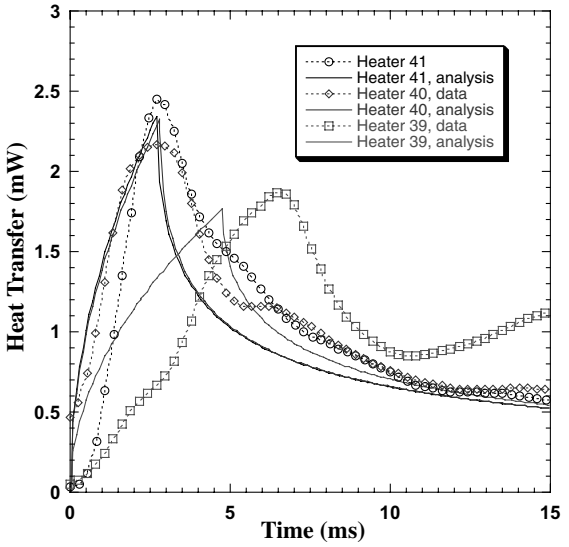

Fig. 14. Comparison of transient conduction calculation with wall heat transfer data.

to the somewhat nonuniform rewetting velocity. The peak heat flux and general trends are captured well, however.

5.2. Circular contact line

Assume the dry patch under a bubble has initial radius r_0 and this dry patch decreases in size allowing liquid to rewet the surface, as might occur just before bubble departure or during bubble oscillation. The time at which radius r becomes wetted with liquid, $t = f(r)$, is assumed to be known from measurements. At time t, a position $r' < r_0$ has been wetted for time $t - t'$. The heat flux at r' is

$$\dot{q}'' = \frac{k(T_w - T_l)}{\sqrt{\pi\alpha_l}} \frac{1}{\sqrt{t - t'}} \tag{14}$$

and the wall heat transfer at time t is

$$\dot{q} = \int_{r_0}^{r} \frac{k(T_w - T_l)}{\sqrt{\pi\alpha_l}} \frac{2\pi r' \, dr'}{\sqrt{f(r) - f(r')}} \tag{15}$$

For the special case where the dry patch diameter shrinks linearly with time ($r = r_0 - vt$), the wall heat transfer can be shown to be

$$\begin{aligned} \dot{q} &= \frac{4\pi k(T_w - T_l)\sqrt{v}}{\sqrt{\pi\alpha_l}} \left[\frac{1}{3}(r_0 - r)^{3/2} + r(r_0 - r)^{1/2} \right] \\ &= \frac{4\pi k(T_w - T_l)\sqrt{v}}{\sqrt{\pi\alpha_l}} \left[\frac{1}{3}(vt)^{3/2} + (r_0 - vt)(vt)^{1/2} \right] \end{aligned} \tag{16}$$

A maximum in heat transfer occurs at time $t = r_0/2v$ and position $r = r_0/2$.

Consider the case where a dry patch radius decreases according to a cosine function $r = r_0 \cos(2\pi ft) + r_i$. This function can be used as a fit to the advancing front location for the data in Fig. 11. The wall heat transfer when the contact line is at position $r_i < r < r_0$ is given by

$$\dot{q} = \int_{r_0}^{r} \frac{k(T_w - T_l)}{\sqrt{\pi\alpha_l}} \times \frac{2\pi r' \, dr'}{\sqrt{\frac{1}{2\pi f}\left[\cos^{-1}\left(\frac{r - r_i}{r_0}\right) - \cos^{-1}\left(\frac{r - r_i}{r_0}\right) \right]}} \tag{17}$$

Comparison between the measured heat transfer and the prediction from the analysis for the data between 8.6 ms $< t <$ 10.5 ms is shown in Fig. 15, and is typical of the results obtained at other times. The change in radius is well fitted by a cosine function. The heat transfer predicted from the conduction analysis is much larger than the measured values. It may not seem possible that the measured heat transfer can be lower than that for transient conduction since any convection or contact line heat transfer should *increase* the wall heat transfer above that for transient conduction. However, it is possible that the liquid rewetting the wall is not from the bulk but from the superheated layer surrounding the bubble, resulting in a smaller $(T_w - T_l)$ and heat transfer than predicted by the analysis. A temperature difference approximately 20% of the wall-to-bulk temperature difference would be required for agreement between the predicted and measured heat transfer at 10.5 ms, consistent with the conclusion of Yaddanapuddi and Kim [9] and Demiray and Kim [10]). The development of a

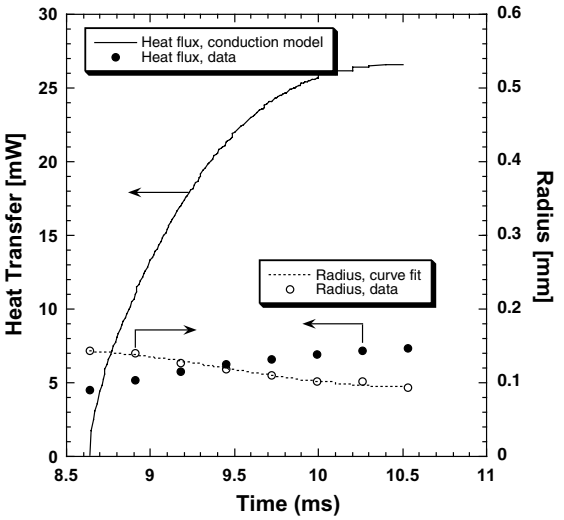

Fig. 15. Comparison of measured heat transfer with transient conduction analysis, and measured radius with the curve fit.

superheated liquid layer around the bubble due to bubble oscillation was discussed earlier.

6. Conclusions

A microheater array was used to obtain time and space resolved wall heat transfer data under nucleating bubbles with low and high subcooling. Single bubbles departing the surface gained the majority of their energy from the superheated liquid layer and not from the wall, indicating that microlayer and contact line heat transfer are not significant. Transient conduction/microconvection was the dominant mechanism for bubble heat transfer. Heat transfer measurements and comparison with a simple model under sliding and oscillating bubbles also indicated that transient conduction during the rewetting process is dominant.

Acknowledgements

This work was sponsored by the Office of Biological and Physical Research at NASA under NCC3-783. Mr. John McQuillen was the grant monitor.

References

[1] V.C. Carey, Liquid–Vapor Phase Change Phenomena, Taylor and Francis (1992).
[2] B.B. Mikic, W.M. Rosenhow, Bubble growth rates in non-uniform temperature field, Prog. Heat Mass Transfer II (1969) 283–292.
[3] M.G. Cooper, A.J.P. Lloyd, The microlayer in nucleate boiling, Int. J. Heat Mass Transfer 12 (1969) 895–913.
[4] P. Stephan, J. Hammer, New model for nucleate boiling heat transfer, Heat Mass Transfer/Waerme Stoffuebertragung 30 (2) (1995) 119–125.
[5] J. Mitrovic, Flow and heat transfer in the wedge-shaped liquid film formed during the growth of a vapour bubble, Int. J. Heat Mass Transfer 41 (12) (1998) 1771–1785.
[6] S.W. Welch, Direct simulation of vapor bubble growth, Int. J. Heat Mass Transfer 41 (1998) 1655–1666.
[7] G. Son, V.K. Dhir, N. Ramanujapu, Dynamics and heat transfer associated with a single bubble during nucleate boiling on a horizontal surface, J. Heat Transfer 121 (1999) 623–631.
[8] Yoon, Koshizuka, Oka, Direct calculation of bubble growth, departure and rise in nucleate boiling, Int. J. Multiphase Flow 27 (2001) 277–298.
[9] N. Yaddanapudi, J. Kim, Single bubble heat transfer in saturated pool boiling of FC-72, Multiphase Sci. Technol. 12 (3–4) (2001) 47–63.
[10] Demiray, Kim, Heat transfer from a single nucleation site during saturated pool boiling of FC-72 using an array of 100 micron heaters, in: Proceedings of the 2002 AIAA/ASME Joint Thermophysics Conference, St. Louis, MO, 2002.
[11] T.D. Rule, J. Kim, Heat transfer behavior on small horizontal heaters during pool boiling of FC-72, J. Heat Transfer 121 (2) (1999) 386–393.
[12] S. Bae, J. Kim, M.H. Kim, Improved technique to measure time and space resolved heat transfer under single bubbles during saturated pool boiling of FC-72, Exp. Heat Transfer 12 (3) (1999).
[13] 3M Corporation, 3M Fluorinert Liquids Product and Contact Guide, 1995.
[14] H.K. Forster, R. Grief, Heat transfer to a boiling liquid-mechanisms and correlations, J. Heat Transfer 81 (1959) 45.